High-Frequency Voltage-Injection Methods and Observer Design for Initial Position Detection of Permanent Magnet Synchronous Machines

Jin, Xinhai; Ni, Ronggang; Chen, Wei; Blaabjerg, Frede; Xu, Dianguo

Published in:
IEEE Transactions on Power Electronics

DOI (link to publication from Publisher):
10.1109/TPEL.2017.2773094

Publication date:
2018

Document Version
Accepted author manuscript, peer reviewed version

High Frequency Voltage Injection Methods and Observer Design for Initial Position Detection of Permanent Magnet Synchronous Machines

Xinhai Jin, Ronggang Ni, *Member*, *IEEE*, Wei Chen, Frede Blaabjerg, *Fellow*, *IEEE*, and Dianguo Xu, *Fellow*, *IEEE*

***Abstract* — The information of the initial rotor position is essential for smooth start up and robust control of Permanent Magnet Synchronous Machines (PMSMs). RoTating Voltage Injection (RTVI) methods in the stationary reference frame have been commonly adopted to detect the initial rotor position at standstill without any position sensors. However, although the Pulsating sqUare-wave Voltage Injection (PUVI) method performs better in estimation time and accuracy, it is rarely used because the estimation result may converge to the q-axis. In this paper, this fault convergence is avoided by modifying the initial states of the position observer, and the PUVI method can finally be used for robust initial rotor position detection. Modified signal processing techniques are proposed for both RTVI and PUVI methods for better implementations in fixed point processors and easier observer gain designs. Detailed comparisons between these two methods are provided. Furthermore, two position estimation observers, i.e. the Proportional–Integral (PI) observer and the Extended State Observer (ESO) are compared, and their parameter tuning methods are studied as well. Both simulation and experimental results are provided for verifications.**

***Index Terms* — Initial rotor position detection, observer, permanent magnet synchronous machine (PMSM), position sensorless control, square-wave voltage injection.**

I. Introduction

PERMANENT magnet synchronous machines (PMSMs) have shown better dynamic performance and higher efficiency compared with induction machines (IMs), and the high performance control strategy such as Field Oriented Control (FOC) is the key to achieve such advantages [1-3]. During FOC, the exact rotor position is required since its initial state, and hence the accurate detection of the PMSM initial rotor position is essential.

Traditionally, the rotor is forced to an intended rotor position before starting up, or started with an open-loop control from standstill to the speed at which the rotor position can be reliably estimated by the ElectroMotive Force (EMF) model based position sensorless control algorithm [4-6]. Both methods disturb the rotor position from standstill, which is prohibited in many applications such as draw benches, electric vehicles, and elevators, etc. Therefore, an accurate and fast initial rotor position detection at standstill is necessary and more practical.

In fact, initial rotor position detection is very much like the position sensorless control at low speed, both of which utilize the anisotropic distribution of the magnetic field in the PMSMs, and detect the saliency by injecting additional signals such as high frequency voltages [7-12]. The main difference between these two procedures is whether the initial rotor position is known. For the position sensorless control adopting high frequency voltage injection methods, the position is estimated near the positive d-axis, which is previously obtained by the initial rotor position detection. Otherwise, the estimated position might converge to the negative d-axis or even the q-axis, which is one of the main problems to be solved.

Two stages are usually taken for the initial position detection. At the first stage, the possible d-axis is observed from excited high frequency signals. Most commonly, rotating voltage injection in the stationary reference frame is applied, which may be either continues injection [13-16] or discrete injection with three pulses [17-18] or twelve pulses [19]. Alternatively, the pulsating sinusoidal voltage injection in the estimated d-axis is also studied [20-21]. In [22], no injection but an additional vibration sensor is used to detect the rotor position.

At the second stage, the polarity of the estimated d-axis is verified. Usually, two pulse voltages with the same magnitudes and injection periods but opposite directions are injected along with the estimated d-axis to detect the difference in saturation [23-24]. Alternatively, the second-order harmonics generated by the injected voltage can be utilized when the pulse sinusoidal voltage is injected [20].

Although various types of injections have been adopted, the pulsating square-wave voltage injection, which has been proved to be the best injection type for low speed position sensorless control [25], can rarely be found for the initial position detection. This is because the initial rotor position estimated from such injection may not only converge to the positive or the negative d-axis, but also to the q-axis which is the unstable equilibrium point [26]. In this paper, a disturbance is manually introduced by setting the initial state a non-zero value in order to avoid the fault convergence. To minimize the voltage injection errors, an improved pulsating square-wave voltage injection method is adopted [12], and modified signal processing techniques are proposed for better implementations

Manuscript received June 4, 2017; revised August 22, 2017; accepted November 1, 2017. (*Corresponding author*: *Ronggang Ni*).

X. Jin is with the School of Electrical Engineering and Automation, Harbin Institute of Technology, Harbin 150001, and the Shanghai STEP Electric Corporation, Shanghai 201802, China (e-mail: 13818863645@139.com).

R. Ni and W. Chen are with the Shanghai STEP Electric Corporation, Shanghai 201802, China (e-mail: ron4ni@163.com, cwmailcn@163.com).

F. Blaabjerg is with the Department of Energy Technology, Aalborg University, Aalborg 9220, Denmark (e-mail: fbl@et.aau.dk).

D. Xu is with the School of Electrical Engineering and Automation, Harbin Institute of Technology, Harbin 150001, China (e-mail: xudiang@hit.edu.cn)

Color versions of one or more of the figures in this paper are available online at http://ieeexplore.ieee.org.

in fixed point digital processors and easier observer gain designs.

Besides injection, the position observer is also significant for fast and robust detection. The Proportional–Integral (PI) observer is the simplest and also very effective [20]. However, the observer bandwidth can be enhanced if the higher order state variable is considered, i.e. the torque. Therefore, the traditional or modified Luenberger observers [27-29] are studied to estimate the disturbance torque as a feedforward compensation. The Luenberger observers are basically Proportional–Integral–Derivative (PID) controllers, where the derivative operation may introduce large noise and it is difficult to tune the controller parameters. In the recent decade, a novel observer named as the Extended State Observer (ESO) is widely studied [30-32], which considers that the highest state variable of a system remains constant at small time scales. The greatest advantage of the ESO is that it contains no derivative but only integral terms. In this paper, the ESO is studied and compared with the PI observer, and their parameter tuning methods are derived.

This paper is organized as follows. Firstly, the most commonly used rotating voltage injection method and the improved pulsating square-wave voltage injection method for initial position detections are investigated, and modified signal processing techniques for both methods are proposed. Secondly, the PI observer and the ESO for position estimations are introduced, and their parameter tuning methods are discussed. Then in Section IV, comprehensive simulation results are provided to prove the above derivations. Finally, experiments on a 5.5 kW PMSM are carried out for further verifications.

II. Rotating and Pulsating Injection Methods for Initial Rotor Position Detections

This section provides detailed derivations of the relationship between the excited high frequency current and the estimated rotor position. Both rotating and improved pulsating square-wave voltage injection methods are discussed for comparisons, and their injection control schemes are shown as the blue and the red blocks in Fig. 1, respectively. Besides, detailed signal processing techniques are proposed to better implement the methods in fixed point processors. Before that, define the average and differential inductances as

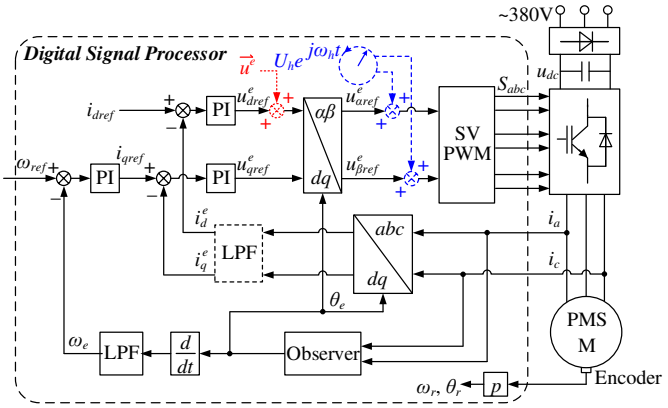

Fig. 1. Control system scheme adopting high frequency voltage injection methods.

$$L_0^r = \left(L_d^r + L_q^r\right)/2, \quad L_1^r = \left(L_d^r - L_q^r\right)/2 \tag{1}$$

where L_d^r and L_q^r are the d- and q-axis inductances in the rotating reference frame, respectively.

Define the position estimation error as

$$\tilde{\theta}_e = \theta_e - \theta_r \tag{2}$$

where θ_e and θ_r are the estimated and the real rotor positions, respectively.

A. Rotating Voltage Injection Method

When a rotating voltage vector with a constant magnitude U_h and a high electric angular velocity ω_h is injected as

$$\overrightarrow{v_{\alpha\beta h}} = v_{\alpha h} + jv_{\beta h} = U_h e^{j\omega_h t} \tag{3}$$

the excited differential current vector can be obtained as (4) where the resistance and the rotating voltage drops are neglected compared with those across the inductances.

$$\begin{aligned}\frac{d\overrightarrow{i_{\alpha\beta h}}}{dt} &= \frac{1}{L_0^{r2} - L_1^{r2}}\left[L_0^r - L_1^r e^{j2(\theta_r - \omega_h t)}\right]\overrightarrow{v_{\alpha\beta h}} \\ &= \frac{U_h}{L_0^{r2} - L_1^{r2}}\left[L_0^r e^{j\omega_h t} - L_1^r e^{j(2\theta_r - \omega_h t)}\right]\end{aligned} . \tag{4}$$

In the steady state, the real and the imaginary components of (4) can be solved as

$$\begin{cases} i_{\alpha h} = \dfrac{U_h/\omega_h}{L_0^{r2} - L_1^{r2}}\left[L_0^r \sin\left(\omega_h t\right) + L_1^r \sin\left(2\theta_r - \omega_h t\right)\right] \\ i_{\beta h} = -\dfrac{U_h/\omega_h}{L_0^{r2} - L_1^{r2}}\left[L_0^r \cos\left(\omega_h t\right) + L_1^r \cos\left(2\theta_r - \omega_h t\right)\right] \end{cases} \tag{5}$$

which can be obtained by processing the sampled α- and β-axis currents with digital Band-Pass Filters (BPFs).

Apply the dot product of the solved current in (5) with a pair of rotating orthogonal vectors, we have

$$\begin{cases} \varepsilon_{h1} = i_{\alpha h}\cos\left(2\theta_e - \omega_h t\right) + i_{\beta h}\sin\left(2\theta_e - \omega_h t\right) \\ \quad = \dfrac{U_h/\omega_h}{L_0^{r2} - L_1^{r2}}\left[L_0^r \sin\left(2\omega_h t - 2\theta_e\right) - L_1^r \sin\left(2\tilde{\theta}_e\right)\right] \\ \varepsilon_{h2} = i_{\alpha h}\sin\left(2\theta_e - \omega_h t\right) - i_{\beta h}\cos\left(2\theta_e - \omega_h t\right) \\ \quad = \dfrac{U_h/\omega_h}{L_0^{r2} - L_1^{r2}}\left[L_0^r \cos\left(2\omega_h t - 2\theta_e\right) + L_1^r \cos\left(2\tilde{\theta}_e\right)\right] \end{cases} . \tag{6}$$

Process the high frequency signals ε_{h1} and ε_{h2} with digital Low-Pass Filters (LPFs), the terms containing the position estimation error can be obtained as

$$\begin{cases} \varepsilon_{n1} = LPF\left(\varepsilon_{h1}\right) = \dfrac{-L_1^r U_h/\omega_h}{L_0^{r2} - L_1^{r2}}\sin\left(2\tilde{\theta}_e\right) \\ \varepsilon_{n2} = LPF\left(\varepsilon_{h2}\right) = \dfrac{L_1^r U_h/\omega_h}{L_0^{r2} - L_1^{r2}}\cos\left(2\tilde{\theta}_e\right) \end{cases} . \tag{7}$$

Normally, only ε_{n1} in (7) is used to observe the rotor position. However, since the inductances, injected voltage magnitude and frequency vary with different machines and controllers, the magnitude of (7) also differs a lot, which may cause data overflow of the following observer in fixed point processors, and increase the difficulty in observer gain designs. Be-

sides, the inverter nonlinearity such as the dead time effect degrades the accuracy of the injected voltage. This is the reason why a pair of orthogonal vectors are used in (6). With the help of (6), the normalized expression containing only the position estimation error can be obtained as

$$\varepsilon_n = \frac{\varepsilon_{n1}}{\sqrt{{\varepsilon_{n1}}^2 + {\varepsilon_{n2}}^2}} = \sin\left(2\tilde{\theta}_e\right). \tag{8}$$

Note that L_1^r is negative.

Although the proposed normalization procedure takes more time for calculations, it is still recommended for the protection of data overflow in fixed point processors and easier observer parameter designs since the gain of ε_n is always unity no matter how the inductances change or the dead time affects. Besides, the extra time needed by the calculations does not matter much during the initial rotor position detection since no other algorithms such as the speed loop control or the FOC, etc. are enabled.

Processing (8) with a PI observer, the electric angular velocity ω_e can be estimated, and the rotor position can be obtained from an integrator. The whole signal processing procedure is shown in Fig. 2.

Note that when (8) is regulated to zero with negative ε_{n2}, $\tilde{\theta}_e$ can be either 0 or 180 eDeg, which means the polarity of the estimated d-axis is uncertain. Therefore, two additional pulse voltages with the same magnitudes and periods but opposite directions need to be injected in the estimated d-axis, and the current slopes are sampled. The larger current slope indicates a smaller inductance and hence more saturation in the d-axis. Therefore, the inject direction with the larger excited current is the positive d-axis.

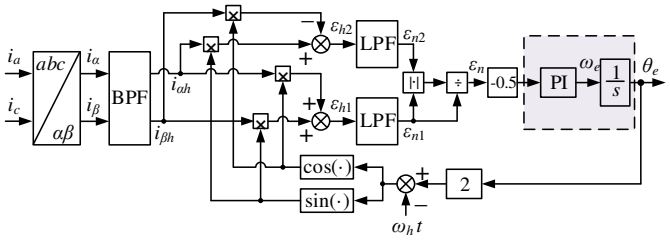

Fig. 2. Signal processing diagram of the rotating voltage injection method for the initial rotor position detection of PMSMs.

B. Improved Pulsating Voltage Injection Method

Although the rotating voltage injection method with the normalized signal processing technique is easy to be implemented in digital systems and robust to voltage injection errors, there are still several drawbacks of this method, which mainly are

1) The estimation error is inevitable because of the neglected transient procedure at the beginning of injection. Note that (5) is obtained only at steady state.
2) More estimation time is needed because of the lower injection frequency.

In fact, all these drawbacks are caused by the type of injected voltage. If the pulsating square-wave voltage is injected, the transient procedure is utilized instead of being neglected, and less filters are needed, which can help to improve the estimation accuracy. Besides, the injection frequency can be increased in order to reduce the estimation time.

To minimize the effects caused by voltage injection errors, the injection type proposed in [12] is used, and a sequence of pulsating square-wave voltages are injected in the estimated d-axis as

$$\overrightarrow{u_{dq}^e} = \begin{cases} +U_h & k = 3n+1 \\ -U_h & k = 3n+2 \\ 0 & k = 3n+3 \end{cases} \tag{9}$$

where k is the control cycles, n = 0, 1, 2, …and increases along with time.

The excited differential current vector in the estimated d- and q-axis is

$$\begin{aligned} \frac{\Delta\overrightarrow{i_{dq}^e}}{\Delta t} &= \frac{L_0^r \overrightarrow{u_{dq}^e} - L_1^r e^{-j2\tilde{\theta}_e} \overrightarrow{u_{dq}^e}^*}{{L_0^r}^2 - {L_1^r}^2} \\ &= \frac{L_0^r - L_1^r \cos\left(2\tilde{\theta}_e\right)}{{L_0^r}^2 - {L_1^r}^2} u_d^e + j\frac{L_1^r \sin\left(2\tilde{\theta}_e\right)}{{L_0^r}^2 - {L_1^r}^2} u_d^e \end{aligned} \tag{10}$$

where Δt is the sampling period, superscript * is the conjugate operator, and the resistance and the rotating voltage drops are neglected.

In [12], only the estimated q-axis current of (10) is utilized to extract the position estimation error as

$$\Delta i_{q\_p}^e - \Delta i_{q\_n}^e = \frac{2L_1^r U_h \Delta t}{{L_0^r}^2 - {L_1^r}^2} \cdot \sin\left(2\tilde{\theta}_e\right) \tag{11}$$

where $\Delta i_{q\_p}^e$ and $\Delta i_{q\_n}^e$ are the q-axis current variations in the estimated reference frame generated by the positive and the negative injections, i.e. $k = 3n+1$ and $k = 3n+2$, respectively.

However, as mentioned in the previous section, (11) makes it difficult to design the observer gains, and may cause data overflow of the following observer in fixed point processors. Therefore, in this paper, a measurement reference frame which lags the estimated reference frame by π/4 is built, shown as the d^m-q^m and the d^e-q^e reference frames respectively in Fig. 3. The d^r-q^r is the real rotor d- and q-axis reference frame with d^r aligned with the N-pole. The superscript s refers to the stationary reference frame. Then the injected voltage in the measurement reference frame is

$$\overrightarrow{u_{dq}^m} = e^{j\frac{\pi}{4}} \overrightarrow{u_{dq}^e} \tag{12}$$

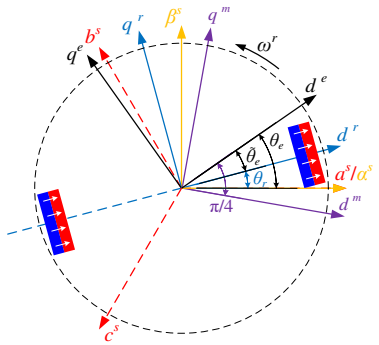

Fig. 3. Different reference frames for rotor position estimation.

and the corresponding differential current vector is

$$\frac{\Delta\overrightarrow{i_{dq}^{m}}}{\Delta t}=\frac{L_0^r\overrightarrow{u_{dq}^{m}}-L_1^r e^{j\left(\frac{\pi}{2}-2\tilde{\theta}_e\right)}\overrightarrow{u_{dq}^{m}}^{*}}{L_0^{r2}-L_1^{r2}}=\frac{L_0^r e^{j\frac{\pi}{4}}-L_1^r e^{j\left(\frac{\pi}{4}-2\tilde{\theta}_e\right)}}{L_0^{r2}-L_1^{r2}}u_d^e \quad (13)$$

Both the d- and q-axis currents in the measurement reference frame are used to detect the current slopes as

$$\begin{cases}\Delta i_{d\_pn}^m=\Delta i_{d\_p}^m-\Delta i_{d\_n}^m\\ \quad=\dfrac{\sqrt{2}U_h\Delta t}{L_0^{r2}-L_1^{r2}}\left[L_0^r-L_1^r\cos\left(2\tilde{\theta}_e\right)-L_1^r\sin\left(2\tilde{\theta}_e\right)\right]\\ \Delta i_{q\_pn}^m=\Delta i_{q\_p}^m-\Delta i_{q\_n}^m\\ \quad=\dfrac{\sqrt{2}U_h\Delta t}{L_0^{r2}-L_1^{r2}}\left[L_0^r-L_1^r\cos\left(2\tilde{\theta}_e\right)+L_1^r\sin\left(2\tilde{\theta}_e\right)\right]\end{cases} \quad (14)$$

where $\Delta i_{d\_p}^m$ and $\Delta i_{q\_p}^m$ are the d- and q-axis current variations in the measurement reference frame generated by the positive injections, i.e. $k = 3n+1$. $\Delta i_{d\_n}^m$ and $\Delta i_{q\_n}^m$ are the d- and q-axis current variations in the measurement reference frame generated by the negative injections, i.e. $k = 3n+2$.

Similarly, the normalized position estimation error can be obtained as

$$\varepsilon_n=\frac{\Delta i_{d\_pn}^m-\Delta i_{q\_pn}^m}{\sqrt{\Delta i_{d\_pn}^{m\ 2}+\Delta i_{q\_pn}^{m\ 2}}}=\frac{\left(L_q^r-L_d^r\right)\sin\left(2\tilde{\theta}_e\right)}{\sqrt{\left(L_0^{r2}+L_1^{r2}\right)-2L_0^rL_1^r\cos\left(2\tilde{\theta}_e\right)}} \quad (15)$$

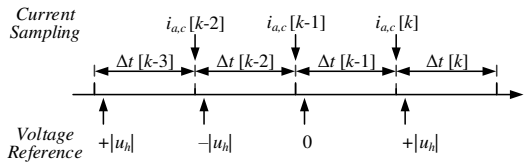

(a)

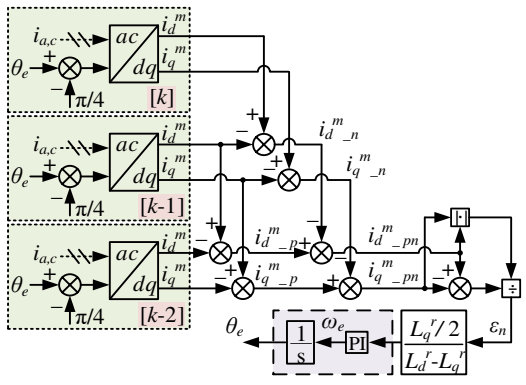

(b)

Fig. 4. Implementation diagram of the improved pulsating square-wave voltage injection method for the initial rotor position detection of PMSMs. (a) Injection and sampling sequences in digital control systems. (b) Signal processing diagram.

When $\tilde{\theta}_e \to 0$ or π,

$$\varepsilon_n \to \left(1-L_d^r/L_q^r\right)\cdot\sin\left(2\tilde{\theta}_e\right) \quad (16)$$

When $\tilde{\theta}_e \to \pm\pi/2$,

$$\varepsilon_n \to \left(L_q^r/L_d^r-1\right)\cdot\sin\left(2\tilde{\theta}_e\right) \quad (17)$$

The injection and sampling sequence, along with the signal processing diagram are shown in Fig. 4. Note that the reference voltage is executed in the next sampling period in digital control systems.

It can be seen from (17) that ε_n can be zero even when the observed result converges to the q-axis, which definitely is unacceptable. However, $\tilde{\theta}_e = \pm\pi/2$ are the unstable equilibrium points. Therefore, to avoid the undesirable convergence especially when the initial position happens to be ± π/2, the initial state of the observer should be set to a non-zero value in order to manually introduce a disturbance.

III. Parameter Tuning and Comparison of the Position Observers

In the previous section, the PI observer is used to estimate the rotor position for both injection methods, which forms a second-order closed loop transfer function. In this section, a third-order observer which is also an Extended State Observer (ESO) is introduced and compared with the PI observer, and their parameter tuning methods are discussed.

A. Parameter Tuning of the PI Observer

When $\tilde{\theta}_e \to 0$, the block diagram adopting the PI observer for position estimation can be drawn as shown in Fig. 5, and the system closed loop transfer function can be written as

$$\Omega_{PI}=\frac{K_p s+K_i}{s^2+K_p s+K_i}. \quad (18)$$

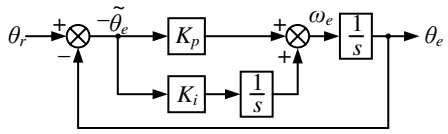

Fig. 5. Block diagram of the PI observer for the position estimation.

For this typical second-order transfer function, let

$$k_P=2\zeta\omega_n,\quad k_I=\omega_n^2 \quad (19)$$

Then ω_n can be solved by letting $\left|\Omega_{PI}\right|_{s=j\omega_{3dB}}=1/\sqrt{2}$ as

$$\omega_n=\omega_{3dB}\sqrt{\sqrt{\left(2\zeta^2+1\right)^2+1}-\left(2\zeta^2+1\right)} \quad (20)$$

where ω_{3dB} is the system bandwidth, and ζ is the damping coefficient, which is usually selected to be larger than 0.707.

B. Parameter Tuning of the ESO

In the PI observer, only position and speed are considered as the state variables. However, for a real mechanical system, the speed is affected by the net torque, which is actually a higher order term. If the net torque can be estimated as a feedforward compensation in the observer, faster convergence can be achieved.

The Luenberger observer has been widely studied for the net torque estimation, which is actually a PID or PIID controller. However, the derivative operation introduces large noise, and it is difficult to tune the parameters.

Alternatively, since the control period is much smaller than the mechanical time constant, the load torque which is actually the high order derivative term of the system can be regarded invariant, and hence its differentiation is zero. At this point of view, the observer can simply be written as third-order state equations as given in (21), where T_{em} is the electromagnetic torque, T_{eL} is the estimated load torque and J is the inertia.

$$\begin{cases} \varepsilon = \theta_e - \theta_r \approx \sin(\theta_e - \theta_r) \\ \dot{\theta}_e = \omega_e - k_{p1}\varepsilon \\ \dot{\omega}_e = \dfrac{p}{J}(T_{em} + T_{eL}) - k_{p2}\varepsilon \\ \dot{T}_{eL} = -\dfrac{J}{p}k_{p3}\varepsilon \end{cases} \cdot \tag{21}$$

The block diagram of the observer in (21) can be drawn as shown in Fig. 6, where it can be seen that only integrators exist and no differentiators are needed.

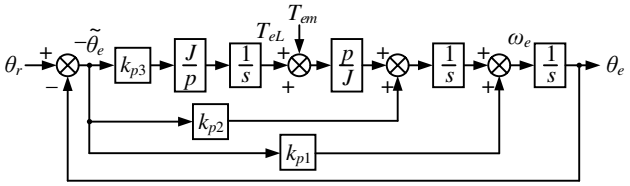

Fig. 6. Block diagram of the ESO for the position estimation.

The Laplace transformation of (21) can be written as

$$\begin{cases} s\theta_e = \omega_e - k_{p1}(\theta_e - \theta_r) \\ s\omega_e = \dfrac{p}{J}T_{eL} - k_{p2}(\theta_e - \theta_r) \\ sT_{eL} = -\dfrac{J}{p}k_{p3}(\theta_e - \theta_r) \end{cases} \tag{22}$$

and the closed loop transfer function can be derived as

$$\Omega_{ESO} = \frac{k_{p1}s^2 + k_{p2}s + k_{p3}}{s^3 + k_{p1}s^2 + k_{p2}s + k_{p3}}. \tag{23}$$

For this typical third-order transfer function, similarly, let

$$k_{p1} = 3\omega_n,\ k_{p2} = 3\omega_n^2,\ k_{p3} = \omega_n^3 \tag{24}$$

and it can be calculated that for $\left|\Omega_{ESO}\right|_{s=j\omega_{3dB}} = 1/\sqrt{2}$,

$$\omega_n = 0.25648\omega_{3dB}. \tag{25}$$

To improve the dynamic performance of (23), the gains in (24) are usually modified with some damping as

$$k_{p1} = (2\zeta+1)\omega_n,\ k_{p2} = (2\zeta+1)\omega_n^2,\ k_{p3} = \omega_n^3 \tag{26}$$

which is named as ESO_C1 for a later comparison.

Alternatively, this paper proposes another modification as

$$k_{p1} = 3\zeta^2\omega_n,\ k_{p2} = 3\zeta\omega_n^2,\ k_{p3} = \omega_n^3 \tag{27}$$

which is named as ESO_C2 for comparison.

C. Comparison among Different Position Observers

The root loci of the PI observer, the ESO with the parameters configured as (26) and (27) are drawn with respect to the damping coefficient ζ as shown in Fig. 7, where the bandwidths, i.e. the parameters defined as ω_{3dB}, are all set as 2π rad/s. It can be seen that for $\zeta > 0$, the PI observer and ESO_C1 are stable. For the stability of ESO_C2, ζ should be larger than 0.481, and normally ζ is set larger than 5.

The bode diagrams of the three observers are drawn in Fig. 8, where ω_{3dB} and ζ are all set as 2π rad/s and 5, respectively. It can be seen the ESO especially with the proposed parameter tuning method as given in (27) has the largest bandwidth. The larger bandwidth indicates a faster convergence and hence less estimation time, but may introduce larger estimation noise and error.

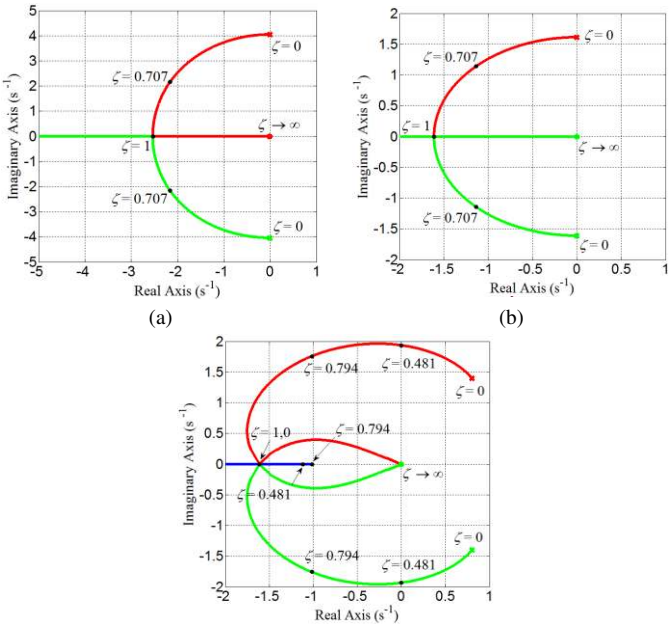

Fig. 7. Root loci of different observers with respect of ζ when ω_{3dB} is configured as 2π rad/s. (a) PI observer with parameter configured as (19). (b) ESO_C1 with parameter configured as (26). (c) ESO_C2 with parameter configured as (27).

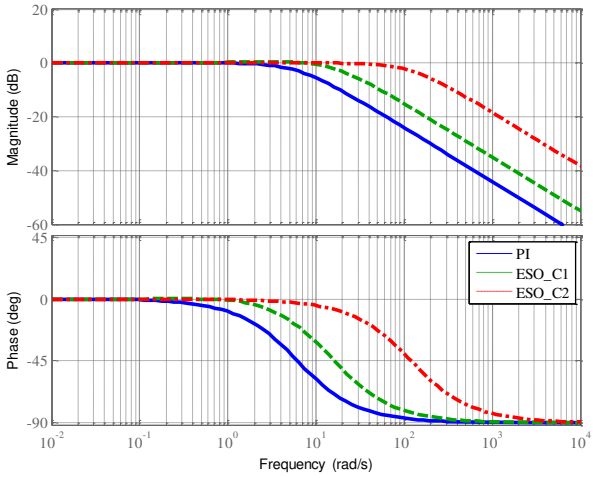

Fig. 8. Bode diagram comparison of different observers with $\zeta = 5$ and $\omega_{3dB} = 2\pi$ rad/s.

IV. Simulation Verifications

Simulink models are built to implement the rotating and the pulsating square-wave voltage injection methods for the initial rotor position detections, where ideal switches are used for the inverter to eliminate the dead time effect, and the linear PMSM model with the parameters listed in Table I is used as the prototype. The implementation of different algorithms is coded in an S-Function in order to be in agreement with the program for experiments, and the digital delays are also included. The PWM switching frequency is set as 5 kHz for a shorter simulation time and a simulation step with exact division, and the sampling and control frequencies are 10 kHz. The simulation step time is set as 0.4 μs, which is 1/500 of the PWM carrier period. During simulation, the PMSM rotor is held at a series of given initial positions from 0 to 360 eDeg, and the estimated initial position waveforms are recorded.

It has been shown in (15) that the estimated initial rotor position adopting the improved pulsating square-wave voltage injection method may not only converge to the d-axis, but also to the q-axis, which is verified in Fig. 9. To solve this problem, the initial states of the observers (18) and (23) are initialized with non-zero values so that to manually introduce some disturbance to the observers.

Fig. 10 shows the estimated positions and the errors at different given positions adopting the rotating voltage injection method with the PI observer. Since the linear PMSM model is used, the rotor polarity cannot be detected, and the estimation converges to the negative d-axis between 110 eDeg and 290 eDeg, covering a region of 180 eDeg, as the red parts of the simulated results show. The position estimation error neglecting the fault estimation of polarity varies from -9.6 eDeg to -6.5 eDeg, and the average value is -8.45 eDeg.

Fig. 11 and Fig. 12 show the estimated positions and the errors at different given positions adopting the improved pulsating square-wave voltage injection method with the PI observer and the ESO, respectively. Similarly, the red parts of the curves represent convergences to the negative d-axis, which also cover half of the electric circle. It can be seen from both figures that the average errors neglecting the fault estimation of polarity are 0 eDeg and 1.4 eDeg, respectively, which are much smaller than that in Fig. 10, and the variations of estimation errors at different given positions are also reduced a lot.

Furthermore, it can be seen that the estimation error adopting the ESO is larger than that adopting the PI observer. However, the convergence time adopting the ESO is much smaller, as shown in Fig. 13. In order to draw a fair comparison, the criteria of convergence are defined as follows.

1) For the rotating voltage injection method, the convergence criterion is defined so that $|\varepsilon_n|$ remains smaller than sin(2×2.5 eDeg) for 20 ms continuously.
2) For the improved pulsating square-wave voltage injection method, the convergence criterion is defined so that $|\varepsilon_n|$ remains smaller than $(1 - L_d^r/L_q^r)\cdot\sin(2\times2.5$ eDeg) for 20 ms continuously.

Both criteria indicate that the position estimation error remains less than a threshold value for a continuous period. Therefore, the minimum convergence time will not be less than the predefined 20 ms, which contains 200 sampling periods.

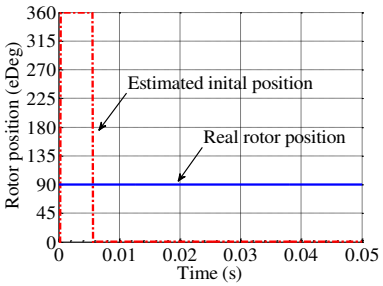

Fig. 9. Initial rotor position estimation at 90 eDeg adopting the improved pulsating square-wave voltage injection method when initial states are set as zero, where the estimated position converges to the q-axis.

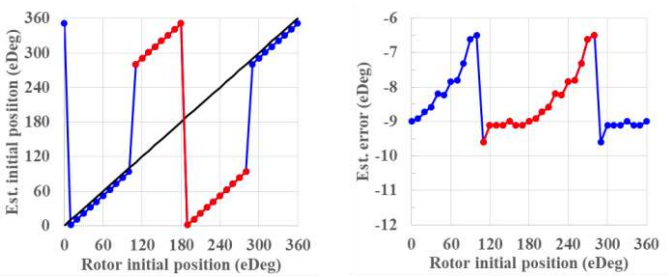

(a) (b)

Fig. 10. Initial position estimation adopting the rotating voltage injection method with the PI observer. (a) Estimated initial rotor position. (b) Estimation error.

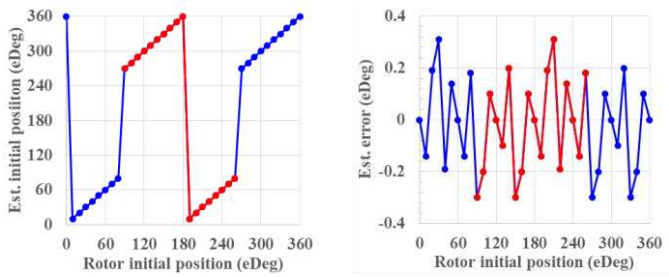

(a) (b)

Fig. 11. Initial position estimation adopting the improved pulsating square-wave voltage injection method with the PI observer. (a) Estimated initial rotor position. (b) Estimation error.

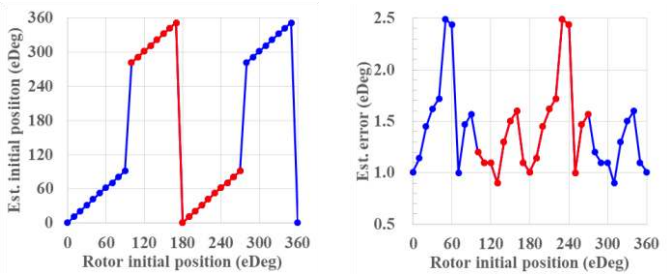

(a) (b)

Fig. 12. Initial position estimation adopting the improved pulsating square-wave voltage injection method with the ESO and parameters configured as (27). (a) Estimated initial rotor position. (b) Estimation error.

Although a higher bandwidth is helpful to reduce the rise time of response, the large oscillation makes it fail to meet the defined convergence criteria. Therefore, bandwidths are chosen for both the fast response and the small oscillation. For the rotating voltage injection method with the PI observer, which is abbreviated as RTVI_PI, the bandwidth is set as 62.8 rad/s.

For the pulsating voltage injection methods with PI and ESO_C2 observers, which are abbreviated as PUVI_PI and PUVI_ESO, the bandwidths are set as 628 rad/s and 157 rad/s, respectively. From Fig. 13, it can be seen that the improved pulsating square-wave voltage injection method converges much faster than the rotating voltage injection method, and the ESO further helps reduce the convergence time.

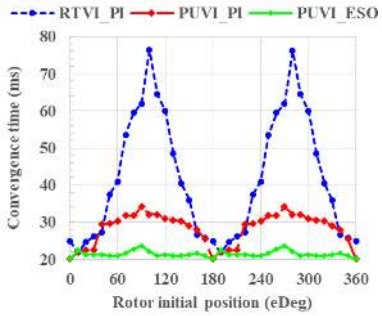

Fig. 13. Convergence time comparison among different voltage injection methods and position observers.

V. Experimental Results

Experiments are carried out on a 5.5 kW PMSM with parameters listed in Table I, and the experiment platform is shown in Fig. 14. A commercial 7.5 kW STEP AS500 inverter is used for voltage injections and samplings. The low-cost fixed point digital processor STM32F103 is used to implement the discussed algorithms. The PWM carrier frequency is set as 1 kHz because of the hardware limitation by the STEP inverters, where an RC filter with the cut-off frequency of only 4.8 kHz is fixed in the AD sampling circuit and cannot be modified. The current sampling and control frequencies are also 1 kHz. An incremental encoder with 1024 pulses per revolution is used to obtain the real rotor position during estimations, and no brakes are used to hold the rotor at standstill.

TABLE I
PARAMETERS OF THE PMSM PROTOTYPE

Rated power	5.5 kW	R_s	0.961 Ω
Rated current	11 A	$L_d{}^r$	17.8 mH
Rated speed	1500 r/min	$L_q{}^r$	78.4 mH
Pole pairs	2	ψ_f	0.741 Wb
Rated torque	35 N·m	J	0.1 kg·m^2

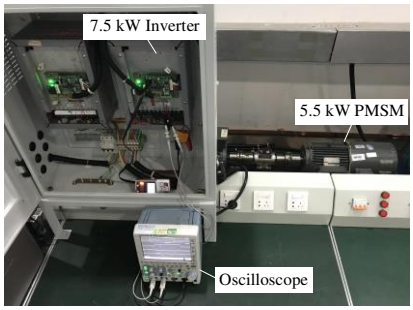

Fig. 14. Experiment platform.

During experiments, the rotor is firstly forced to a preset position by injecting a constant voltage vector, which is set as the initial position for the incremental encoder. When the induced current attenuates to zero, either the rotating or the improved pulsating voltage injection method with the PI observer is performed to estimate the rotor position. Then the polarity is detected by injecting a pair of opposite voltage vectors. The overall procedure for experiments is shown in Fig. 15. The convergence criteria are similar to those adopted in simulations, but the threshold of the estimation error is set as 5 eDeg instead of 2.5 eDeg, and the continuous period is extended up to 100 ms.

The experimental waveforms adopting the rotating and the improved pulsating voltage injection methods are shown in Fig. 16 and Fig. 17 respectively, where from top to bottom are the flag for time counting, position estimation error, i.e. $\tilde{\theta}_e$, and the phase A current. The estimation flag waveforms show the time consumed by the voltage injection methods and polarity detections respectively, between which is the time for the phase current attenuation.

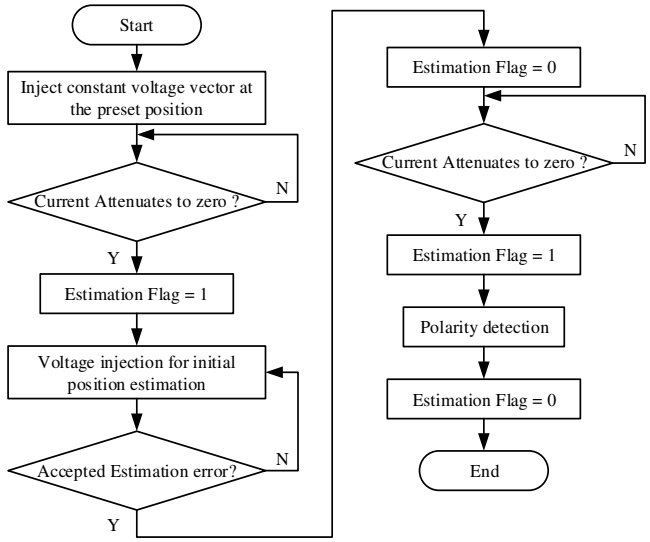

Fig. 15. Procedures taken during experiments.

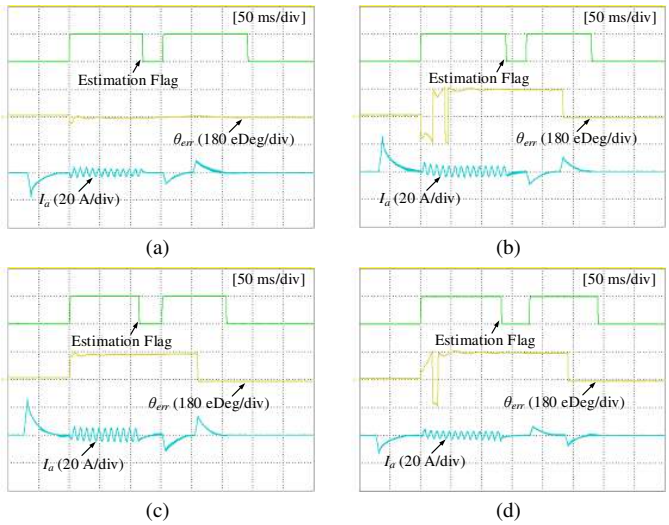

Fig. 16. Experimental waveforms of the rotating voltage injection method at different preset initial positions. (a) At 50 eDeg. (b) At 150 eDeg. (c) At 210 eDeg. (d) At 310 eDeg.

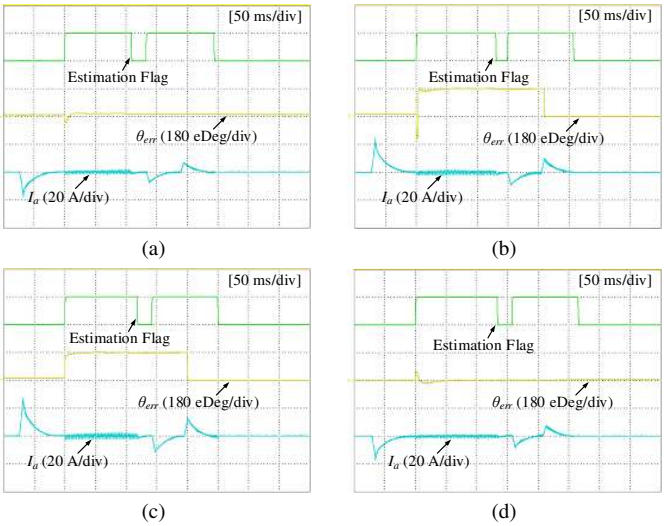

Fig. 17. Experimental waveforms of the improved pulsating square-wave voltage injection method at different preset initial positions. (a) At 50 eDeg. (b) At 150 eDeg. (c) At 210 eDeg. (d) At 310 eDeg.

It can be seen from the waveforms that the improved pulsating voltage injection method has a faster response and more accurate estimation results, which is in accordance with the simulation results. Besides, the excited current adopting the improved voltage injection method is much smaller than that excited by the rotating injection with the same injected voltage magnitude, which is beneficial to noise reduction and loss minimization.

VI. Conclusion

In this paper, the improved pulsating square-wave voltage injection method is investigated for the initial rotor position detection of PMSMs. The initial state of the estimated speed is set to a non-zero value in order to prevent the fault convergence to the q-axis. Position estimation error normalization techniques are proposed for both the pulsating and the rotating voltage injection methods in order to be better implemented in fixed point processors and easier for the observer gain design. The parameter tuning methods for both the PI observer and the ESO are studied, and the ESO shows larger bandwidth and position estimation error compared with the PI observer. Comprehensive simulation and experimental results verify that the improved pulsating square-wave voltage injection method performs faster and more accurate compared with the rotating voltage injection method.

References

[1] P. E. Kakosimos, A. G. Sarigiannidis, M. E. Beniakar, A. G. Kladas, and C. Gerada, "Induction Motors Versus Permanent-Magnet Actuators for Aerospace Applications," *IEEE Trans. Ind. Electron.,* vol. 61, no. 8, pp. 4315-4325, 2014.

[2] R. Ni, D. Xu, G. Wang, L. Ding, G. Zhang, and L. Qu, "Maximum Efficiency Per Ampere Control of Permanent-Magnet Synchronous Machines," *IEEE Trans. Ind. Electron.,* vol. 62, no. 4, pp. 2135-2143, 2015.

[3] R. Ni, D. Xu, G. Wang, X. Gui, G. Zhang, H. Zhan, and C. Li, "Efficiency Enhancement of General AC Drive System by Remanufacturing Induction Motor with Interior Permanent-Magnet Rotor," *IEEE Trans. Ind. Electron.,* vol. 63, no. 2, pp. 808-820, 2016.

[4] R. Wu, and G. R. Slemon, "A Permanent Magnet Motor Drive without a Shaft Sensor," *IEEE Trans. Ind. Appl.,* vol. 27, no. 5, pp. 1005-1011, 1991.

[5] N. Matsui, "Sensorless Operation of Brushless DC Motor Drives," in *Proceedings of the IEEE IECON'93*, 1993, pp. 739-744.

[6] N. Matsui, "Sensorless PM Brushless DC Motor Drives," *IEEE Trans. Ind. Electron.,* vol. 43, no. 2, pp. 300-308, 1996.

[7] M. Schroedl, "Operation of the Permanent-Magnet Synchronous Machine without a Mechanical Sensor," in *Proceedings of the Fourth International Conference on Power Electronics and Variable-Speed Drives*, London, 1990, pp. 51-56.

[8] P. L. Jansen, and R. D. Lorenz, "Transducerless Position and Velocity Estimation in Induction and Salient AC Machines," *IEEE Trans. Ind. Appl.,* vol. 31, no. 2, pp. 240-247, 1995.

[9] M. J. Corley, and R. D. Lorenz, "Rotor Position and Velocity Estimation for a Salient-Pole Permanent Magnet Synchronous Machine at Standstill and High Speeds," *IEEE Trans. Ind. Appl.,* vol. 34, no. 4, pp. 784-789, 1998.

[10] R. Masaki, S. Kaneko, M. Hombu, T. Sawada, and S. Yoshihara, "Development of a Position Sensorless Control System on an Electric Vehicle Driven by a Permanent Magnet Synchronous Motor," in *Proceedings of the Power Conversion Conference (PCC-Osaka 2002)*, 2002, pp. 571-576.

[11] S.-K. Sul, and S. Kim, "Sensorless Control of IPMSM: Past, Present, and Future," *IEEJ Journal of Industry Applications,* vol. 1, no. 1, pp. 15-23, 2012.

[12] R. Ni, D. Xu, F. Blaabjerg, K. Lu, G. Wang, and G. Zhang, "Square-Wave Voltage Injection Algorithm for PMSM Position Sensorless Control With High Robustness to Voltage Errors," *IEEE Trans. Power Electron.,* vol. 32, no. 7, pp. 5425-5437, 2017.

[13] M. E. Haque, Z. Limin, and M. F. Rahman, "A Sensorless Initial Rotor Position Estimation Scheme for a Direct Torque Controlled Interior Permanent Magnet Synchronous Motor Drive," *IEEE Trans. Power Electron.,* vol. 18, no. 6, pp. 1376-1383, 2003.

[14] K. Hyunbae, H. Kum-Kang, R. D. Lorenz, and T. M. Jahns, "A Novel Method for Initial Rotor Position Estimation for IPM Synchronous Machine Drives," *IEEE Trans. Ind. Appl.,* vol. 40, no. 5, pp. 1369-1378, 2004.

[15] J. Yu-seok, R. D. Lorenz, T. M. Jahns, and S. Seung-Ki, "Initial Rotor Position Estimation of an Interior Permanent-Magnet Synchronous Machine Using Carrier-Fequency Injection Methods," *IEEE Trans. Ind. Appl.,* vol. 41, no. 1, pp. 38-45, 2005.

[16] J. Hu, J. Liu, and L. Xu, "Eddy Current Effects on Rotor Position Estimation and Magnetic Pole Identification of PMSM at Zero and Low Speeds," *IEEE Trans. Power Electron.,* vol. 23, no. 5, pp. 2565-2575, 2008.

[17] M. Boussak, "Implementation and Experimental Investigation of Sensorless Speed Control with Initial Rotor Position Estimation for Interior Permanent Magnet Synchronous Motor Drive," *IEEE Trans. Power Electron.,* vol. 20, no. 6, pp. 1413-1422, 2005.

[18] Y. Wang, N. Guo, J. Zhu, N. Duan, S. Wang, Y. Guo, W. Xu, and Y. Li, "Initial Rotor Position and Magnetic Polarity Identification of PM Synchronous Machine Based on Nonlinear Machine Model and Finite Element Analysis," *IEEE Trans. Magn.,* vol. 46, no. 6, pp. 2016-2019, 2010.

[19] S. Nakashima, Y. Inagaki, and I. Miki, "Sensorless Initial Rotor Position Estimation of Surface Permanent-Magnet Synchronous Motor," *IEEE Trans. Ind. Appl.,* vol. 36, no. 6, pp. 1598-1603, 2000.

[20] H. Jung-Ik, K. Ide, T. Sawa, and S. Seung-Ki, "Sensorless Rotor Position Estimation of an Interior Permanent-Magnet Motor from Initial States," *IEEE Trans. Ind. Appl.,* vol. 39, no. 3, pp. 761-767, 2003.

[21] W. Sun, J. X. Shen, M. J. Jin, and H. Hao, "A Robust Magnetic Polarity Self-Sensing Method for Start Up of PM Synchronous Machine in Fan-like System," *IEEE Trans. Ind. Appl.,* vol. 53, no. 3, pp. 2169-2177, 2017.

[22] S. Pekarek, and P. Beccue, "Using Torque-Ripple-Induced Vibration to Determine the Initial Rotor Position of a Permanent Magnet Synchronous Machine," *IEEE Trans. Power Electron.,* vol. 21, no. 3, pp. 818-821, 2006.

[23] T. Noguchi, K. Yamada, S. Kondo, and I. Takahashi, "Initial Rotor Position Estimation Method of Sensorless PM Synchronous Motor with no Sensitivity to Armature Resistance," *IEEE Trans. Ind. Electron.,* vol. 45, no. 1, pp. 118-125, 1998.

[24] J. Holtz, "Acquisition of Position Error and Magnet Polarity for Sensorless Control of PM Synchronous Machines," *IEEE Trans. Ind. Appl.,* vol. 44, no. 4, pp. 1172-1180, 2008.

[25] Y.-D. Yoon, S.-K. Sul, S. Morimoto, and K. Ide, "High-Bandwidth Sensorless Algorithm for AC Machines Based on Square-Wave-Type

Voltage Injection," *IEEE Trans. Ind. Appl.,* vol. 47, no. 3, pp. 1361-1370, 2011.

[26] H. Zhaobin, Y. Linru, and W. Zhaodong, "Sensorless Initial Rotor Position Identification for Non-Salient Permanent Magnet Synchronous Motors Based on Dynamic Reluctance Difference," *IET Power Electronics,* vol. 7, no. 9, pp. 2336-2346, 2014.

[27] K. Hyunbae, M. C. Harke, and R. D. Lorenz, "Sensorless Control of Interior Permanent-Magnet Machine Drives with Zero-Phase Lag Position Estimation," *IEEE Trans. Ind. Appl.,* vol. 39, no. 6, pp. 1726-1733, 2003.

[28] Y. D. Yoon, E. Jung, A. Yoo, and S. K. Sul, "Dual Observers for the Disturbance Rejection of a Motion Control System," in *Proceedings of the 42nd IEEE Industry Applications Annual Meeting*, 2007, pp. 256-261.

[29] S.-C. Yang, and R. D. Lorenz, "Surface Permanent-Magnet Machine Self-Sensing at Zero and Low Speeds Using Improved Observer for Position, Velocity, and Disturbance Torque Estimation," *IEEE Trans. Ind. Appl.,* vol. 48, no. 1, pp. 151-160, 2012.

[30] J. Han, "From PID to Active Disturbance Rejection Control," *IEEE Trans. Ind. Electron.,* vol. 56, no. 3, pp. 900-906, 2009.

[31] A. A. Godbole, J. P. Kolhe, and S. E. Talole, "Performance Analysis of Generalized Extended State Observer in Tackling Sinusoidal Disturbances," *IEEE Trans. Contr. Syst. T.,* vol. 21, no. 6, pp. 2212-2223, 2013.

[32] J. Yao, Z. Jiao, and D. Ma, "Adaptive Robust Control of DC Motors With Extended State Observer," *IEEE Trans. Ind. Electron.,* vol. 61, no. 7, pp. 3630-3637, 2014.

Xinhai Jin received the B.S. degree in Automation from Qingdao University, Qingdao, China in 2001, and the M.S. degree in Control Engineering from Tongji University, Shanghai, China in 2010.

Since 2001, he has been with the Shanghai STEP Electric Corporation, Shanghai, China, where he is now the vice CEO of STEP and the Dean of the STEP Research Center.

Mr. Jin is also currently working toward the Ph.D. degree in Electrical Engineering at Harbin Institute of Technology, Harbin, China. His research interests include inverter drive systems and intelligent control.

Ronggang Ni (S'14–M'17) received the B.S., M.S. and Ph.D. degrees from Harbin Institute of Technology, Harbin, China, in 2010, 2012 and 2017, respectively, all in Electrical Engineering.

From September 2015 to September 2016, he was a Visiting Scholar at the Department of Energy Technology, Aalborg University, Denmark. Since 2017, he has been with the Shanghai STEP Electric Corporation, Shanghai, China, where he is currently working as an engineer. His research interests include analysis and design of electric machines for high efficiency and high power density applications, and the related control technics with emphases on high efficiency, high dynamic and position sensorless control.

Dr. Ni is an active reviewer for IEEE sponsored conferences and several IEEE top journals.

Wei Chen received the B.S. degree in Automation Control from Central South University, Changsha, China, in 2005, and the M.S. and Ph.D. degrees in Electrical Engineering from Harbin Institute of Technology (HIT), Harbin, China, in 2007 and 2012 respectively.

In 2012, he joined Shanghai STEP Electric Corporation. He is now manager of R&D Dept., and the Vice Dean of Central Research Institute in STEP Co. His research interests include sensorless vector controlled motor drives, high performance PMSM servo system. He published 16 technical papers.

Frede Blaabjerg (S'86–M'88–SM'97–F'03) was with ABB-Scandia, Randers, Denmark, from 1987 to 1988. From 1988 to 1992, he got the PhD degree in Electrical Engineering at Aalborg University in 1995. He became an Assistant Professor in 1992, an Associate Professor in 1996, and a Full Professor of power electronics and drives in 1998. From 2017 he became a Villum Investigator.

His current research interests include power electronics and its applications such as in wind turbines, PV systems, reliability, harmonics and adjustable speed drives. He has published more than 500 journal papers in the fields of power electronics and its applications. He is the co-author of two monographs and editor of 6 books in power electronics and its applications.

He has received 24 IEEE Prize Paper Awards, the IEEE PELS Distinguished Service Award in 2009, the EPE-PEMC Council Award in 2010, the IEEE William E. Newell Power Electronics Award 2014 and the Villum Kann Rasmussen Research Award 2014. He was the Editor-in-Chief of the IEEE TRANSACTIONS ON POWER ELECTRONICS from 2006 to 2012. He has been Distinguished Lecturer for the IEEE Power Electronics Society from 2005 to 2007 and for the IEEE Industry Applications Society from 2010 to 2011 as well as 2017 to 2018.

He is nominated in 2014, 2015, 2016 and 2017 by Thomson Reuters to be between the most 250 cited researchers in Engineering in the world. In 2017 he became Honoris Causa at University Politehnica Timisoara (UPT), Romania.

Dianguo Xu (M'97–SM'12–F'17) received the B.S. degree in control engineering from Harbin Engineering University, Harbin, China, in 1982, and the M.S. and Ph.D. degrees in electrical engineering from the Harbin Institute of Technology (HIT), Harbin, in 1984 and 1989, respectively.

In 1984, he joined the Department of Electrical Engineering, HIT, as an Assistant Professor. Since 1994, he has been a Professor with the Department of Electrical Engineering, HIT. He was the Dean of School of Electrical Engineering and Automation, HIT, from 2000 to 2010, and was the Assistant President of HIT from 2010 to 2014. He is currently the Vice President of HIT. His current research interests include renewable energy generation technology, power quality mitigation, sensorless vector controlled motor drives, high performance servo system. He has authored or co-authored over 600 technical papers. Prof. Xu serves as an Associate Editor for the IEEE TRANSACTIONS ON INDUSTRIAL ELECTRONICS and the IEEE JOURNAL OF EMERGING AND SELECTED TOPICS IN POWER ELECTRONICS. He also serves as the Chairman of the IEEE Harbin Section.